Available online at www.sciencedirect.com

ScienceDirect

IFAC PapersOnline CONFERENCE PAPER ARCHIVE

IFAC PapersOnLine 58-16 (2024) 95–100

Kalman Filter as Observer and Smoother for Rigid-Body Motion Control Applications ⋆

Joel Reis * **Carlos Silvestre** *,**

* *Faculty of Science and Technology, University of Macau, Macao, China (e-mail: joelreis@um.edu.mo,csilvestre@um.edu.mo).*

** *Institute for Systems and Robotics, Instituto Superior Técnico, Universidade de Lisboa, 1049-001 Lisboa, Portugal.*

Abstract: This paper addresses the problem of estimating non measured quantities in rigid body motion control applications resorting to Kalman filter theory. These quantities include the linear velocity of the rigid body, and external force and torque disturbances applied to its center of mass. The set of sensor measurements (pose and angular velocity readings) is noise-filtered as well. The overall framework consists of a linear time-varying system, shown to be uniformly completely observable, and an exponentially stable nonlinear controller. Simulation results are presented to validate and showcase the attainable performance of the proposed methodology.

Keywords: Rigid body motion control, Kalman filter, Observability, Exogenous disturbances

1. INTRODUCTION

The celebrated Kalman filter (KF) remains as arguably one of the most important tools for state estimation and for measurement noise filtering since its inception Kalman (1960). Indeed, for the past six decades, the KF and its variants have found applications across virtually all fields of science, as extensively reported in Urrea and Agramonte (2021), where it is emphasized that the main advantages of the KF and its variants are their simplicity and capability to provide accurate estimations and prediction results. In the 1980s, the KF was already recognized as a fundamental tool for aerospace systems Schmidt (1981); Shuster (1989), where attitude filtering and estimation is a critical mission aspect. Interestingly, despite its long-established history, researchers continue to improve on KF-based methodologies, and to develop new applications. Among a vast literature, we find in Markley and Sedlak (2008) a seven-parameter angular-momentum-based representation that is shown to be advantageous for attitude estimation of spinning spacecraft, while the work in Aravkin et al. (2017) presents a tutorial on convex optimization techniques applied to state estimation using KF. More recently, the work in Vouch et al. (2024) proposes a customized trajectory-aware extended KF architecture to overcome issues of reduced GNSS signal availability and poor geometry by leveraging external aiding data.

We note that state estimation in general, and estimation of unknown quantities in particular, is not only motivated by the lack of sensors that can directly measure state variables, but also by sensor inaccuracies in the control feedback loop, e.g., bias offsets, installation misalignment, and ongoing changes in accuracy characteristics of measuring instruments that are not known in advance Afonin et al. (2020). Besides, filtering of sensor noise is also critical for an accurate and smooth performance of robust controllers. Within the scope of KF theory, linear-quadratic-Gaussian (LQG) controllers have been a staple of optimal control theory regarding linear systems driven by Gaussian noise, and, to some extent, nonlinear systems with near-linear characteristics. LQG controllers may have less popularity in aircraft/spacecraft applications, but the literature still offers many contributions to choose from. For instance, an LQG robust controller is described in Chrif and Kadda (2014) for the lateral and longitudinal flight dynamics of an aircraft control system, and in Zarei et al. (2007) two robust controllers are designed and compared for a vertical short take-off and landing aircraft system.

LQG controllers are simple to implement and offer a reasonable performance, although they are generally not robust when the model itself or its parameters contain some degree of uncertainty. Moreover, to accommodate extra features like integral action and disturbance rejection, the system plant must be augmented by taking into account a model of the disturbance. In robotics, researchers often resort to active disturbance rejection control (ADRC) techniques to deal with the presence of (internal and external) perturbations. A comprehensive review on the application of ADRC approaches is presented in Fareh et al. (2021).

The *regular* KF is often seen as a tool exclusive to linear systems. Because of that, its variations have drawn a lot of attention in tackling highly nonlinear problems based on specific topological constructions. For instance, Mangiacapra et al. (2022) proposes an integrated stochastic

⋆ This work was supported in part by the Macau Science and Technology Development Fund under Grant FDCT/0192/2023/RIA3, in part by the University of Macau, Macau, China, under Projects MYRG-GRG2023-00107-FST-UMDF and MYRG2022-00205-FST, and Conference Grant CG-FST-2024, and in part by the Fundação para a Ciência e a Tecnologia (FCT), Portugal through ISR LARSyS-FCT Project under Grant UIDB/50009/2020.

10.1016/j.ifacol.2024.08.468

estimation and tracking control on Lie groups and their tangent bundles in a precise, asymptotically stable navigation and control system that considers the orbit-attitude coupling in the presence of stochasticity. Similarly, the seminal work in Barrau and Bonnabel (2017) analyzes the convergence aspects of the invariant extended KF when it is used as a deterministic nonlinear observer on Lie groups.

In this paper, we show that despite the inherent nonlinearity associated with the equations describing the general motion of a rigid body, it is possible, in most practical scenarios, to use a linear KF, with no linearization involved, to obtain estimates of non measured quantities, specifically linear velocity and exogenous perturbations affecting the linear and angular dynamics, as well as to obtain noise-filtered measurements from the available sensors. Our KF is then combined with a nonlinear controller to demonstrate a robust and accurate pose tracking performance in the context of navigation of spacecraft/aircraft systems.

1.1 Notation

The set of real numbers is denoted by $\mathbb{R}$. The n-dimensional Euclidean space is denoted by $\mathbb{R}^n$. The symbol $\mathbf{0}_{m\times n}$ (resp. $\mathbf{0}_m$) denotes an $m\times n$ (resp. $m\times m$) matrix of zeros and $\mathbf{I}_m$ an $m\times m$ identity matrix. The superscript $(\bullet)^\mathsf{T}$ denotes the transpose operator. The set of unit vectors on $\mathbb{R}^3$ is denoted by $\mathbb{S}^2$. The special orthogonal group of order three is denoted by $\mathsf{SO}(3) := \{\mathbf{M}\in\mathbb{R}^{3\times3} : \mathbf{M}\mathbf{M}^\mathsf{T} = \mathbf{M}^\mathsf{T}\mathbf{M} = \mathbf{I}_3\ ,\ \det(\mathbf{M}) = +1\}$. We define (the skew-symmetric operator) $\mathbf{S}(\bullet)$ such that $\mathbf{a}\times\mathbf{b} = \mathbf{S}(\mathbf{a})\mathbf{b}$, for $\mathbf{a},\mathbf{b}\in\mathbb{R}^3$. The inverse map associated with $\mathbf{S}(\bullet)$ is denoted by vex, e.g., $\mathrm{vex}(\mathbf{S}(\mathbf{a})) = \mathbf{a}$. For $\mathbf{M}\in\mathbb{R}^{m\times n}$, we let $\mathrm{vec}(\mathbf{M})$ return an mn-dimensional column vector obtained by stacking the columns of $\mathbf{M}$. For $\mathbf{x}\in\mathbb{R}^n$, the Euclidean norm is given by $\|\mathbf{x}\| := \sqrt{\mathbf{x}^\mathsf{T}\mathbf{x}}$. The Kronecker product is denoted by $\otimes$. The multiple-input operator $\mathrm{blkdiag}(\bullet,\bullet,\dots,\bullet)$ returns a block diagonal matrix, with input matrices aligned along the main diagonal.

2. EQUATIONS OF MOTION FOR A RIGID-BODY

Consider two reference frames: a fixed inertial one, denoted by $\mathcal{I}$; and a body-fixed one, denoted by $\mathcal{B}$, whose origin is located at the center of mass of the rigid body. We define the rotation matrix from $\mathcal{B}$ to $\mathcal{I}$ as $\mathbf{R}\in\mathsf{SO}(3)$. The angular kinematics of the rigid body follows, for all $t\geq t_0\geq 0$, as

$$\dot{\mathbf{R}}(t) = \mathbf{R}(t)\mathbf{S}(\boldsymbol{\Omega}(t)),\quad \mathbf{R}(t_0)\in\mathsf{SO}(3), \tag{1}$$

where $\boldsymbol{\Omega}\in\mathbb{R}^3$ represents the angular velocity of $\mathcal{B}$ with respect to $\mathcal{I}$, expressed in $\mathcal{B}$. Let $\mathbf{p}\in\mathbb{R}^3$ and $\mathbf{v}\in\mathbb{R}^3$ denote the inertial position and velocity, respectively, of a rigid-body. With (1) standing for the angular kinetics of the rigid-body, the linear counterpart is given, for all $t\geq t_0$, by $\dot{\mathbf{p}}(t) = \mathbf{v}(t)$, with initial condition $\mathbf{p}(t_0)\in\mathbb{R}^3$.

The kinetics of a rigid-body undergoing translational and rotational motion are typically written, for all $t\geq t_0$, as

$$\dot{\mathbf{v}}(t) = \mathbf{R}(t)\mathbf{f}(t) + \mathbf{b}_\mathbf{v},\qquad \mathbf{v}(t_0)\in\mathbb{R}^3, \tag{2a}$$

$$\mathbf{J}\dot{\boldsymbol{\Omega}}(t) = -\mathbf{S}(\boldsymbol{\Omega}(t))\mathbf{J}\boldsymbol{\Omega}(t) + \boldsymbol{\tau}(t) + \mathbf{b}_{\boldsymbol{\tau}},\qquad \boldsymbol{\Omega}(t_0)\in\mathbb{R}^3, \tag{2b}$$

where $\mathbf{f}\in\mathbb{R}^3$, expressed in $\mathcal{B}$, is a vector comprised of known forces applied to the rigid body's center of mass, $\mathbf{b}_\mathbf{v}\in\mathbb{R}^3$, expressed in $\mathcal{I}$, represents unknown constant external forces, $\mathbf{J}\in\mathbb{R}^{3\times3}$ is the rigid body inertia matrix, $\boldsymbol{\tau}\in\mathbb{R}^3$, expressed in $\mathcal{B}$, is a vector comprised of known torques applied to the rigid body's center of mass, and, finally, $\mathbf{b}_{\boldsymbol{\tau}}\in\mathbb{R}^3$ represents unknown constant external torques acting on the center of mass of the rigid-body.

Assumption 1. The system input (comprising force $\mathbf{f}(t)$ and torque $\boldsymbol{\tau}(t)$) is uniformly bounded for all $t\geq t_0$.

2.1 Problem Statement

Our goal in this work is threefold: i) to obtain estimates of $\mathbf{v}$, $\mathbf{b}_\mathbf{v}$ and $\mathbf{b}_{\boldsymbol{\tau}}$; ii) to obtain noise-filtered measurements of pose ($\mathbf{p}$ and $\mathbf{R}$) and angular velocity $\boldsymbol{\Omega}$; and iii) to achieve pose tracking based on desired reference curves $\mathbf{p}_d\in\mathbb{R}^3$ and $\mathbf{R}_d\in\mathsf{SO}(3)$, such that $\dot{\mathbf{R}}_d(t) = \mathbf{R}_d(t)\mathbf{S}(\boldsymbol{\Omega}_d(t))$ for all $t\geq t_0$, with $\mathbf{R}_d(t_0)\in\mathsf{SO}(3)$, and where $\boldsymbol{\Omega}_d(t)\in\mathbb{R}^3$.

3. LTV SYSTEM DESIGN

Consider the following rotation matrix decomposition:

$$\mathbf{R}(t)^\mathsf{T} = [\mathbf{r}_1(t)\ \mathbf{r}_2(t)\ \mathbf{r}_3(t)], \tag{3}$$

where $\mathbf{r}_1,\mathbf{r}_2,\mathbf{r}_3\in\mathbb{S}^2$ are orthonormal vectors corresponding to the rows of $\mathbf{R}$. Using (3), we proceed by defining

$$\boldsymbol{\chi}(t) := \mathrm{vec}(\mathbf{R}(t)^\mathsf{T}) = \left[\mathbf{r}_1^\mathsf{T}(t)\ \mathbf{r}_2^\mathsf{T}(t)\ \mathbf{r}_3^\mathsf{T}(t)\right]^\mathsf{T}\in\mathbb{R}^9, \tag{4}$$

such that, according to (1) we have

$$\dot{\boldsymbol{\chi}}(t) = -\left(\mathbf{I}_3\otimes\mathbf{S}(\boldsymbol{\Omega}(t))\right)\boldsymbol{\chi}(t),\ \boldsymbol{\chi}(t_0) := \mathrm{vec}(\mathbf{R}(t_0)). \tag{5}$$

Let us now define a system state vector $\mathbf{x}\in\mathbb{R}^{24}$ as

$$\mathbf{x}(t) := \left[\mathbf{p}(t)^\mathsf{T}\ \mathbf{v}(t)^\mathsf{T}\ \mathbf{b}_\mathbf{v}^\mathsf{T}\ \middle|\boldsymbol{\chi}(t)^\mathsf{T}\middle|\ \boldsymbol{\omega}(t)^\mathsf{T}\ \mathbf{b}_{\boldsymbol{\tau}}^\mathsf{T}\right]^\mathsf{T}. \tag{6}$$

where, for simplicity of notation, we have defined $\boldsymbol{\omega}(t) := \mathbf{J}\boldsymbol{\Omega}(t)\in\mathbb{R}^3$. According to (1), (2) and (6), we are able to synthesize an LTV system (in a noise-free setting) as

$$\begin{cases}\dot{\mathbf{x}}(t) = \mathbf{A}(t)\mathbf{x}(t) + \mathbf{B}(t)\mathbf{u}(t), & \text{(7a)}\\ \mathbf{y}(t) = \mathbf{C}\mathbf{x}(t), & \text{(7b)}\end{cases}$$

where $\mathbf{A}(t)\in\mathbb{R}^{24\times24}$ is defined as

$$\mathbf{A}(t) := \mathrm{blkdiag}(\mathbf{A}_\mathbf{p}, \mathbf{A}_{\boldsymbol{\chi}}(t), \mathbf{A}_{\boldsymbol{\omega}}(t)), \tag{8}$$

with

$$\mathbf{A}_\mathbf{p} := \begin{bmatrix}0&1&0\\0&0&1\\0&0&0\end{bmatrix}\otimes\mathbf{I}_3\in\mathbb{R}^{9\times9}, \tag{9}$$

$$\mathbf{A}_{\boldsymbol{\chi}}(t) := -\mathbf{I}_3\otimes\mathbf{S}(\boldsymbol{\Omega}(t))\in\mathbb{R}^{9\times9} \tag{10}$$

and

$$\mathbf{A}_{\boldsymbol{\omega}}(t) := \begin{bmatrix}-\mathbf{S}(\boldsymbol{\Omega}(t)) & \mathbf{I}_3\\ \mathbf{0}_3 & \mathbf{0}_3\end{bmatrix}\in\mathbb{R}^{6\times6}, \tag{11}$$

where $\mathbf{B}(t)\in\mathbb{R}^{24\times6}$ is the input matrix defined as

$$\mathbf{B}(t) := \left[\begin{array}{cc}\mathbf{0}_3&\mathbf{0}_3\\ \mathbf{R}(t)&\mathbf{0}_3\\ \mathbf{0}_3&\mathbf{0}_3\\ \hline \mathbf{0}_{9\times3}&\mathbf{0}_{9\times3}\\ \hline \mathbf{0}_3&\mathbf{I}_3\\ \mathbf{0}_3&\mathbf{0}_3\end{array}\right]\begin{array}{l}\left.\begin{array}{l}\\\\\end{array}\right\}\mathbf{B}_\mathbf{p}(t)\in\mathbb{R}^{9\times6}\\ \left.\begin{array}{l}\end{array}\right\}\mathbf{B}_{\boldsymbol{\chi}}\in\mathbb{R}^{9\times6}\\ \left.\begin{array}{l}\\\end{array}\right\}\mathbf{B}_{\boldsymbol{\omega}}\in\mathbb{R}^{6\times6}\end{array}, \tag{12}$$

$$\mathbf{u}(t) := \left[\mathbf{f}(t)^\mathsf{T}\ \boldsymbol{\tau}(t)^\mathsf{T}\right]^\mathsf{T}\in\mathbb{R}^6, \tag{13}$$

$$\mathbf{C} := \mathrm{blkdiag}(\mathbf{C}_\mathbf{p}, \mathbf{C}_{\boldsymbol{\chi}}, \mathbf{C}_{\boldsymbol{\omega}})\in\mathbb{R}^{15\times24}, \tag{14}$$

where $\mathbf{C}_\mathbf{p} := [\mathbf{I}_3\ \mathbf{0}_3\ \mathbf{0}_3]\in\mathbb{R}^{3\times9}$, $\mathbf{C}_{\boldsymbol{\chi}} := \mathbf{I}_9$ and $\mathbf{C}_{\boldsymbol{\omega}} := \left[\mathbf{J}^{-1}\ \mathbf{0}_3\right]\in\mathbb{R}^{3\times6}$, and, finally, where

$$\mathbf{y}(t) := \left[\mathbf{p}(t)^\mathsf{T}\middle|\ \boldsymbol{\chi}(t)^\mathsf{T}\middle|\ \boldsymbol{\Omega}(t)^\mathsf{T}\right]^\mathsf{T}\in\mathbb{R}^{15}. \tag{15}$$

3.1 Observability Analysis

The observability of the LTV system (7) is examined here. We begin by noticing that, on account of the structures of $\mathbf{A}(t)$ and $\mathbf{C}$ given in (8) and (14), respectively, the system (7) actually comprises three uncoupled linear sub-systems whose observability we could analyze separately.

Definition 2. (Brockett (2015)). A transformation $\mathbf{z}(t) := \mathbf{T}(t)\mathbf{x}(t)$ is a Lyapunov transformation if, for all $t \geq t_0$:

(i) $\mathbf{T}(t)$ has a continuous derivative.
(ii) $\mathbf{T}(t)$ and its derivative are bounded for all $t \geq t_0$.
(iii) there exists $c > 0$ such that $c \leq |\det(\mathbf{T}(t))|$.

Let us consider the following Lyapunov transformation:

$$\mathbf{z}(t) := \underbrace{\text{blkdiag}(\mathbf{I}_3, \mathbf{I}_3, \mathbf{I}_3, \mathbf{I}_3 \otimes \mathbf{R}(t), \mathbf{R}(t), \mathbf{I}_3)}_{\mathbf{T}(t) \in \mathbb{R}^{24\times 24}} \mathbf{x}(t). \quad (16)$$

The resulting *transformed* LTV system can be written as

$$\begin{cases} \dot{\mathbf{z}}(t) = \boldsymbol{\mathcal{A}}(t)\mathbf{z}(t) + \text{blkdiag}(\mathbf{I}_{18}, \mathbf{R}(t), \mathbf{I}_3)\mathbf{B}(t)\mathbf{u}(t), \\ \mathbf{y}(t) = \boldsymbol{\mathcal{C}}(t)\mathbf{z}(t), \end{cases}$$

where $\boldsymbol{\mathcal{A}}(t) \in \mathbb{R}^{9\times 9}$ is given by

$$\boldsymbol{\mathcal{A}}(t) := \text{blkdiag}\left(\mathbf{A}_\mathbf{p}, \mathbf{0}_9, \begin{bmatrix} \mathbf{0}_3 & \mathbf{R}(t) \\ \mathbf{0}_3 & \mathbf{0}_3 \end{bmatrix}\right), \quad (18)$$

and where $\boldsymbol{\mathcal{C}}(t) \in \mathbb{R}^{15\times 24}$ is given by

$$\boldsymbol{\mathcal{C}}(t) := \text{blkdiag}\left([\mathbf{I}_3 \ \mathbf{0}_{3\times 6}], \mathbf{I}_3 \otimes \mathbf{R}(t)^\mathsf{T}, [\mathbf{J}^{-1}\mathbf{R}(t)^\mathsf{T} \ \mathbf{0}_3]\right). \quad (19)$$

The transformation suggested in (16) not only renders the subsystem concerning the evolution of $\boldsymbol{\chi}$ time-invariant, but also renders the new state transition matrix associated with (11) a nilpotent matrix of degree 2. Moreover, since Lyapunov transformations preserve stability properties, any property derived in the sequel for the *transformed* system (17) also applies to the original LTV system (7).

The transition matrices associated with (9), (10) and (11), following the Lyapunov transformation in (16), are computed via the Peano-Baker series, and denoted here by $\boldsymbol{\Phi}_\mathbf{p}(t, t_0) \in \mathbb{R}^{9\times 9}$, $\boldsymbol{\Phi}_{\boldsymbol{\chi}}(t, t_0) \in \mathbb{R}^{9\times 9}$ and $\boldsymbol{\Phi}_{\boldsymbol{\omega}}(t, t_0) \in \mathbb{R}^{6\times 6}$, respectively. According to (18), they follow as

$$\boldsymbol{\Phi}_\mathbf{p}(t, t_0) = \begin{bmatrix} 1 & t - t_0 & (t - t_0)^2/2 \\ 0 & 1 & t - t_0 \\ 0 & 0 & 1 \end{bmatrix} \otimes \mathbf{I}_3, \quad (20)$$

$$\boldsymbol{\Phi}_{\boldsymbol{\chi}}(t, t_0) = \mathbf{I}_9, \text{ and} \quad (21)$$

$$\boldsymbol{\Phi}_{\boldsymbol{\omega}}(t, t_0) = \begin{bmatrix} \mathbf{I}_3 & \int_{t_0}^{t} \mathbf{R}(\sigma) d\sigma \\ \mathbf{0}_3 & \mathbf{I}_3 \end{bmatrix}. \quad (22)$$

The results in (20), (21) and (22) are easily verified by recalling properties of transition matrices, namely $\dot{\boldsymbol{\Phi}}(t, t_0) = \mathbf{A}(t)\boldsymbol{\Phi}(t, t_0)$ and $\boldsymbol{\Phi}(t_0, t_0) = \mathbf{I}_{24}$, with $\boldsymbol{\Phi}(t, t_0) := \text{blkdiag}(\boldsymbol{\Phi}_\mathbf{p}(t, t_0), \boldsymbol{\Phi}_{\boldsymbol{\chi}}(t, t_0), \boldsymbol{\Phi}_{\boldsymbol{\omega}}(t, t_0)) \in \mathbb{R}^{24\times 24}$.

The observability Gramian associated with $(\boldsymbol{\mathcal{A}}(t), \boldsymbol{\mathcal{C}}(t))$, denoted here by $\boldsymbol{\mathcal{W}}(t_0, t_f) \in \mathbb{R}^{24\times 24}$, is defined as

$$\boldsymbol{\mathcal{W}}(t_0, t_f) := \int_{t_0}^{t_f} \boldsymbol{\Phi}(t, t_0)^\mathsf{T} \boldsymbol{\mathcal{C}}(t)^\mathsf{T} \boldsymbol{\mathcal{C}}(t) \boldsymbol{\Phi}(t, t_0) dt. \quad (23)$$

Definition 3. Jazwinski (1970) Given positive constants α_1, α_2 and β, the continuous-time LTV system (17) is uniformly completely observable (u.c.o.) if and only if

$$\alpha_1 \mathbf{I}_{24} \prec \boldsymbol{\mathcal{W}}(t, t + \beta) \prec \alpha_2 \mathbf{I}_{24}, \quad \forall t \geq t_0. \quad (24)$$

Proposition 4. (Batista et al. (2011)). Let $\mathbf{g}(\tau) : [t, t + \beta] \subset \mathbb{R} \to \mathbb{R}^3$ be a continuous and i-times continuously differentiable function on $\phi := [t, t + \beta]$, where $\beta > 0$, and such that $\mathbf{g}(t) = d\mathbf{g}(t)/dt = \ldots = d^{i-1}\mathbf{g}(t)/dt^{i-1} = \mathbf{0}$. Further assume that there exists $C > 0$ such that $\|d^{i+1}\mathbf{g}(\tau)/d\tau^{i+1}\| \leq C$ for all $\tau \in \phi$. If there exist $\rho > 0$ and $\tau_1 \in \phi$ such that $\|d^i\mathbf{g}(t)/dt^i|_{t=\tau_1}\| \geq \rho$, then there exist $0 < \tau_2 \leq \beta$ and $\theta > 0$ such that $\|\mathbf{g}(t + \tau_2)\| \geq \theta$.

Theorem 5. The continuous-time LTV system (17) is uniformly completely observable on $\phi := [t, t + \beta]$, for $\beta > 0$.

Proof. Based on (24), by setting $t_0 = t$ and $t = t + \beta$ in (23), we obtain the following result:

$$\begin{aligned} \boldsymbol{\mathcal{W}}(t, t + \beta) &= \int_t^{t+\beta} \boldsymbol{\Phi}(\sigma, t)^\mathsf{T} \boldsymbol{\mathcal{C}}(t)^\mathsf{T} \boldsymbol{\mathcal{C}}(t) \boldsymbol{\Phi}(\sigma, t) d\sigma \\ &= \text{blkdiag}(\underbrace{\boldsymbol{\mathcal{W}}_\mathbf{p}(\beta)}_{\in\mathbb{R}^{9\times 9}}, \underbrace{\boldsymbol{\mathcal{W}}_{\boldsymbol{\chi}}(\beta)}_{\in\mathbb{R}^{9\times 9}}, \underbrace{\boldsymbol{\mathcal{W}}_{\boldsymbol{\omega}}(t, t + \beta)}_{\in\mathbb{R}^{6\times 6}}), \end{aligned} \quad (25)$$

where, according to (19), (20) and (21) we have obtained $\boldsymbol{\mathcal{W}}_\mathbf{p}(\beta) := \beta[1 \ \frac{\beta}{2} \ \frac{\beta^2}{6}; \frac{\beta}{2} \ \frac{\beta^2}{3} \ \frac{\beta^3}{8}; \frac{\beta^2}{6} \ \frac{\beta^3}{8} \ \frac{\beta^4}{20}] \otimes \mathbf{I}_3$ and $\boldsymbol{\mathcal{W}}_{\boldsymbol{\chi}}(\beta) := \beta\mathbf{I}_9$. Next, let us define a constant vector $\mathbf{d} := [\mathbf{d}_1^\mathsf{T} \ \mathbf{d}_2^\mathsf{T}]^\mathsf{T}$, with $\mathbf{d}_1, \mathbf{d}_2, \in \mathbb{R}^3$ such that $\|\mathbf{d}\| = 1$. Based on (19) and (22), left and right multiplying $\boldsymbol{\mathcal{W}}_{\boldsymbol{\omega}}(t, t + \beta)$ by $\mathbf{d}$ gives $\mathbf{d}^\mathsf{T}\boldsymbol{\mathcal{W}}_{\boldsymbol{\omega}}(t, t + \beta)\mathbf{d} = \int_t^{t+\beta} \|\mathbf{g}(\tau, t)\|^2 d\tau$ with $\mathbf{g}(\tau, t) \in \mathbb{R}^3$ defined, for all $\tau \in \phi$, and $t \geq t_0$, as

$$\mathbf{g}(\tau, t) := \mathbf{J}^{-1}\mathbf{R}(\tau)\left(\mathbf{d}_1 + \int_t^\tau \mathbf{R}(\sigma)\mathbf{d}_2 d\sigma\right). \quad (26)$$

Recall that $\mathbf{J}$ is a positive definite matrix, meaning that $\underline{\lambda}\mathbf{I}_3 \preceq \mathbf{J} \preceq \overline{\lambda}\mathbf{I}_3$, where $0 \leq \underline{\lambda} \leq \overline{\lambda}$ represent the smallest and largest eigenvalues of $\mathbf{J}$, respectively. Furthermore, since $\mathbf{R}$ is a norm-preserving matrix, we note that, for some $\|\mathbf{d}_1\| = \delta_1 > 0$, it must be, according to (26), $\|\mathbf{g}(t, t)\| \geq \delta_1/\overline{\lambda}$ for all $t \geq t_0$. Suppose then that $\mathbf{d}_1 = \mathbf{0}$, meaning that $\|\mathbf{d}_2\| = 1$. Next, we compute the derivative of (26) with respect to τ, which results in

$$\frac{d\mathbf{g}(\tau, t)}{d\tau} = \mathbf{J}^{-1}\mathbf{R}(\tau)\mathbf{S}(\boldsymbol{\Omega}(\tau)) \int_t^\tau \mathbf{R}(\sigma)\mathbf{d}_2 d\sigma + \mathbf{J}^{-1}\mathbf{d}_2.$$

Note that $\|d\mathbf{g}(\tau, t)/d\tau|_{\tau=t}\| = \|\mathbf{J}^{-1}\mathbf{d}_2\| \geq \underline{\lambda}$ for all $t \geq t_0$. Furthermore, according to *Assumption* 1, and based on (2b), there exists a constant $c_1 > 0$ such that $\|d^2\mathbf{g}(\tau, t)/d\tau^2\| \leq c_1$ for all $\tau \in \phi$. Hence, and based on *Proposition* 4, we conclude from the previous analysis that there always exist positive constants $\bar{\alpha}_1$ and $\bar{\alpha}_2$, function of β, such that $\bar{\alpha}_1(\beta)\mathbf{I}_6 \preceq \boldsymbol{\mathcal{W}}_{\boldsymbol{\omega}}(t, t + \beta) \preceq \bar{\alpha}_2\mathbf{I}_6$, for all $t \geq t_0$ and $\beta > 0$. With $\boldsymbol{\mathcal{W}}_\mathbf{p}(\beta)$ and $\boldsymbol{\mathcal{W}}_{\boldsymbol{\chi}}(\beta)$ already established as positive definite constant matrices whose smallest and largest eigenvalues are only function of β, we conclude, based on (25), that there always exist positive constants α_1 and α_2, function of β, such that $\alpha_1(\beta)\mathbf{I}_{24} \preceq \boldsymbol{\mathcal{W}}(t, t + \beta) \preceq \alpha_2(\beta)\mathbf{I}_{24}$, for all $t \geq t_0$ and $\beta > 0$. In view of *Definition* 3, the LTV system (17) must be u.c.o..

4. KALMAN FILTER AS ESTIMATOR

In this section, we will consider the system dynamics (originally expressed by (7)) in the presence of sensor noise. More specifically, the true output (15) is given by

$$\mathbf{y}_m(t) = \begin{bmatrix} \mathbf{p}_m(t) \\ \boldsymbol{\chi}_m(t) \\ \boldsymbol{\Omega}_m(t) \end{bmatrix} := \begin{bmatrix} \mathbf{p}(t) \\ \boldsymbol{\chi}(t) \\ \boldsymbol{\Omega}(t) \end{bmatrix} + \begin{bmatrix} \mathbf{n}_\mathbf{p}(t) \\ \mathbf{n}_{\boldsymbol{\chi}}(t) \\ \mathbf{n}_{\boldsymbol{\Omega}}(t) \end{bmatrix} \begin{matrix} \} \in \mathbb{R}^3 \\ \} \in \mathbb{R}^9 \\ \} \in \mathbb{R}^3 \end{matrix}, \quad (27)$$

where $\mathbf{n}_{\mathbf{p}}(t) \sim \mathcal{N}(0, \sigma_{\mathbf{p}}^2)$, $\mathbf{n}_{\boldsymbol{\chi}}(t) \sim \mathcal{N}(0, \sigma_{\boldsymbol{\chi}}^2)$ and $\mathbf{n}_{\boldsymbol{\Omega}}(t) \sim \mathcal{N}(0, \sigma_{\boldsymbol{\Omega}}^2)$ are extracted from zero mean multivariate normal distributions with standard deviations $\sigma_{\mathbf{p}}, \sigma_{\boldsymbol{\chi}}, \sigma_{\boldsymbol{\Omega}} > 0$. All sources of noise are assumed uncorrelated.

Then, similarly to (6), let the corresponding system state estimate be denoted by

$$\widehat{\mathbf{x}}(t) := \left[\widehat{\mathbf{p}}(t)^\mathsf{T} \ \widehat{\mathbf{v}}(t)^\mathsf{T} \ \widehat{\mathbf{b}}_{\mathbf{v}}(t)^\mathsf{T} \ \left|\widehat{\boldsymbol{\chi}}(t)^\mathsf{T}\right| \ \widehat{\boldsymbol{\omega}}(t)^\mathsf{T} \ \widehat{\mathbf{b}}_{\boldsymbol{\tau}}(t)^\mathsf{T}\right]^\mathsf{T} \in \mathbb{R}^{24}. \tag{28}$$

Based on (7a) and (7b), we put forward a Kalman-Bucy filter whose state update is computed as (cf. Simon (2006))

$$\dot{\widehat{\mathbf{x}}}(t) := \mathbf{A}(t)\widehat{\mathbf{x}}(t) + \mathbf{B}(t)\mathbf{u}(t) + \boldsymbol{\mathcal{K}}(t)(\mathbf{y}_m(t) - \mathbf{C}\widehat{\mathbf{x}}(t)), \tag{29}$$

with $\mathbf{A}$, $\mathbf{B}$, $\mathbf{C}$ as given in (8), (12) and (14), respectively, and where $\boldsymbol{\mathcal{K}} \in \mathbb{R}^{24\times 15}$ is the Kalman gain computed as

$$\boldsymbol{\mathcal{K}}(t) := \boldsymbol{\mathcal{P}}(t)\mathbf{C}^\mathsf{T}\boldsymbol{\mathcal{R}}^{-1}, \tag{30}$$

with $\boldsymbol{\mathcal{P}} \in \mathbb{R}^{24\times 24}$ denoting the (positive-definite) covariance matrix of the state estimate that satisfies the matrix Riccati differential equation governed by

$$\dot{\boldsymbol{\mathcal{P}}}(t) := \mathbf{A}(t)\boldsymbol{\mathcal{P}}(t) + \boldsymbol{\mathcal{P}}(t)\mathbf{A}(t)^\mathsf{T} + \boldsymbol{\mathcal{Q}} - \boldsymbol{\mathcal{K}}(t)\boldsymbol{\mathcal{R}}\boldsymbol{\mathcal{K}}(t)^\mathsf{T}, \tag{31}$$

with $\boldsymbol{\mathcal{P}}(t_0) \succ \mathbf{0}$, and with $\boldsymbol{\mathcal{Q}} \in \mathbb{R}^{24\times 24}$ and $\boldsymbol{\mathcal{R}} \in \mathbb{R}^{15\times 15}$ being the positive-definite covariance matrices of the process and observation noises, respectively. We note that these two matrices characterize different additive white Gaussian noise distributions; they can be seen as tuning knobs for adjusting performance.

Remark 6. Given that the LTV system (7) is comprised of three decoupled LTV subsystems, the 24-dimensional KF given by (29), (30) and (31) may actually be implemented as three separate KFs.

Based on the previous remark, let us consider henceforward $\boldsymbol{\mathcal{P}}(t) = \text{blkdiag}(\boldsymbol{\mathcal{P}}_{\mathbf{p}}(t), \boldsymbol{\mathcal{P}}_{\boldsymbol{\chi}}(t), \boldsymbol{\mathcal{P}}_{\boldsymbol{\omega}}(t))$, with $\boldsymbol{\mathcal{P}}_{\mathbf{p}}, \boldsymbol{\mathcal{P}}_{\boldsymbol{\chi}} \in \mathbb{R}^{9\times 9}$, $\boldsymbol{\mathcal{P}}_{\boldsymbol{\omega}} \in \mathbb{R}^{6\times 6}$, $\boldsymbol{\mathcal{Q}} = \text{blkdiag}(\boldsymbol{\mathcal{Q}}_{\mathbf{p}}, \boldsymbol{\mathcal{Q}}_{\boldsymbol{\chi}}, \boldsymbol{\mathcal{Q}}_{\boldsymbol{\omega}})$, with $\boldsymbol{\mathcal{Q}}_{\mathbf{p}}, \boldsymbol{\mathcal{Q}}_{\boldsymbol{\chi}} \in \mathbb{R}^{9\times 9}$, $\boldsymbol{\mathcal{Q}}_{\boldsymbol{\omega}} \in \mathbb{R}^{6\times 6}$, $\boldsymbol{\mathcal{R}} = \text{blkdiag}(\boldsymbol{\mathcal{R}}_{\mathbf{p}}, \boldsymbol{\mathcal{R}}_{\boldsymbol{\chi}}, \boldsymbol{\mathcal{R}}_{\boldsymbol{\Omega}})$, with $\boldsymbol{\mathcal{R}}_{\mathbf{p}} \in \mathbb{R}^{3\times 3}$, $\boldsymbol{\mathcal{R}}_{\boldsymbol{\chi}} \in \mathbb{R}^{9\times 9}$, $\boldsymbol{\mathcal{R}}_{\boldsymbol{\Omega}} \in \mathbb{R}^3$. Therefore, we may also define $\boldsymbol{\mathcal{K}}_{\mathbf{p}}(t) := \boldsymbol{\mathcal{P}}_{\mathbf{p}}(t)\mathbf{C}_{\mathbf{p}}^\mathsf{T}\boldsymbol{\mathcal{R}}_{\mathbf{p}}^{-1} \in \mathbb{R}^{9\times 3}$, $\boldsymbol{\mathcal{K}}_{\boldsymbol{\chi}}(t) := \boldsymbol{\mathcal{P}}_{\boldsymbol{\chi}}(t)\mathbf{C}_{\boldsymbol{\chi}}^\mathsf{T}\boldsymbol{\mathcal{R}}_{\boldsymbol{\chi}}^{-1} \in \mathbb{R}^{9\times 9}$, $\boldsymbol{\mathcal{K}}_{\boldsymbol{\omega}}(t) := \boldsymbol{\mathcal{P}}_{\boldsymbol{\omega}}(t)\mathbf{C}_{\boldsymbol{\omega}}^\mathsf{T}\boldsymbol{\mathcal{R}}_{\boldsymbol{\Omega}}^{-1} \in \mathbb{R}^{3\times 3}$.

Remark 7. The KF ignores topological constructions. To project $\widehat{\boldsymbol{\chi}}$ back onto $\mathsf{SO}(3)$ one can resort, for instance, to the technique described in (Moakher, 2002, Proposition 3.5), which is based in the singular value decomposition. With $\overline{\mathbf{R}}(t) := \text{vec}^{-1}(\widehat{\boldsymbol{\chi}}(t)) \in \mathbb{R}^{3\times 3}$, it follows that $\widehat{\mathbf{R}}(t) := \overline{\mathbf{R}}(t)\mathbf{U}(t)\text{diag}(\Lambda_1^{-1/2}(t), \Lambda_2^{-1/2}(t), s(t)\Lambda_3^{-1/2}(t))\mathbf{U}(t)$, with $\overline{\mathbf{R}}(t)^\mathsf{T}\overline{\mathbf{R}}(t) = \mathbf{U}(t)^\mathsf{T}\text{diag}(\Lambda_1(t), \Lambda_2(t), \Lambda_3(t))\mathbf{U}(t)$ and $s(t) = 1$ if $\det(\overline{\mathbf{R}}(t) > 0$ or, else, $s(t) = -1$, if $\det(\overline{\mathbf{R}}(t) < 0$.

4.1 State Transition Matrix: On the Robustness to Noise

We must stress that, upon implementing the KF, two of the LTV subsystems incorporate noise-corrupted measurements of angular velocity, i.e., $\boldsymbol{\Omega}_m$, in their state transition matrices, namely (10) and (11). Consequently, noise is also present in the dynamics of the Riccati equation (31). Based on (5) and (27), we may thus write

$$\begin{aligned}\dot{\boldsymbol{\chi}}(t) &= -\mathbf{A}_{\boldsymbol{\chi}}(t)\boldsymbol{\chi}(t) \\ &= -\left(\mathbf{I}_3 \otimes \mathbf{S}(\boldsymbol{\Omega}_m(t))\right)\boldsymbol{\chi}(t) + \left(\mathbf{I}_3 \otimes \mathbf{S}(\mathbf{n}_{\boldsymbol{\Omega}}(t))\right)\boldsymbol{\chi}(t).\end{aligned} \tag{32}$$

Consider now the Lyapunov function

$$V_{\boldsymbol{\chi}}(t) := \widetilde{\boldsymbol{\chi}}(t)^\mathsf{T}\boldsymbol{\mathcal{P}}_{\boldsymbol{\chi}}^{-1}(t)\widetilde{\boldsymbol{\chi}}(t), \tag{33}$$

where we have defined the error $\widetilde{\boldsymbol{\chi}}(t) := \boldsymbol{\chi}(t) - \widehat{\boldsymbol{\chi}}(t) \in \mathbb{R}^9$, such that its derivative, according to (27), (29) and (32), can be computed as follows: $\dot{\widetilde{\boldsymbol{\chi}}}(t) = \dot{\boldsymbol{\chi}}(t) - \dot{\widehat{\boldsymbol{\chi}}}(t) = -\left(\mathbf{I}_3 \otimes \mathbf{S}(\boldsymbol{\Omega}_m(t))\right)\widetilde{\boldsymbol{\chi}}(t) + \left(\mathbf{I}_3 \otimes \mathbf{S}(\mathbf{n}_{\boldsymbol{\Omega}}(t))\right)\boldsymbol{\chi}(t) - \boldsymbol{\mathcal{P}}_{\boldsymbol{\chi}}(t)^\mathsf{T}\boldsymbol{\mathcal{R}}_{\boldsymbol{\chi}}^{-1}(\mathbf{C}\widetilde{\boldsymbol{\chi}}(t) + \mathbf{n}_{\boldsymbol{\Omega}}(t))$. According to (29) and (32), the time derivative of $V_{\boldsymbol{\chi}}(t)$ in (33) can be written as

$$\begin{aligned}\dot{V}_{\boldsymbol{\chi}}(t) = &-\widetilde{\boldsymbol{\chi}}(t)^\mathsf{T}(\boldsymbol{\mathcal{P}}_{\boldsymbol{\chi}}^{-1}(t)\boldsymbol{\mathcal{Q}}_{\boldsymbol{\chi}}\boldsymbol{\mathcal{P}}_{\boldsymbol{\chi}}^{-1}(t) + \boldsymbol{\mathcal{R}}_{\boldsymbol{\chi}}^{-1})\widetilde{\boldsymbol{\chi}} \\ &-\boldsymbol{\chi}(t)^\mathsf{T}\left(\mathbf{I}_3 \otimes \mathbf{S}(\mathbf{n}_{\boldsymbol{\Omega}}(t))\right)\boldsymbol{\mathcal{P}}_{\boldsymbol{\chi}}^{-1}(t)\widetilde{\boldsymbol{\chi}}(t) \\ &+\widetilde{\boldsymbol{\chi}}(t)^\mathsf{T}\boldsymbol{\mathcal{P}}_{\boldsymbol{\chi}}^{-1}(t)\left(\mathbf{I}_3 \otimes \mathbf{S}(\mathbf{n}_{\boldsymbol{\Omega}}(t))\right)\boldsymbol{\chi}(t) \\ &-2\mathbf{n}_{\boldsymbol{\chi}}(t)^\mathsf{T}\boldsymbol{\mathcal{R}}_{\boldsymbol{\chi}}^{-1}\widetilde{\boldsymbol{\chi}}(t).\end{aligned} \tag{34}$$

Finding explicit solutions for (31) is generally impractical. However, let us set $\boldsymbol{\mathcal{P}}_{\boldsymbol{\chi}}(t_0) = r_1\mathbf{I}_9$, $\boldsymbol{\mathcal{Q}}_{\boldsymbol{\chi}} = r_2\mathbf{I}_9$ and $\boldsymbol{\mathcal{R}}_{\boldsymbol{\chi}} = r_3\mathbf{I}_9$ for some $r_1, r_2, r_3 > 0$, which is reasonable for this specific LTV subsystem. Based on (10) and (31), and employing the fact that $\mathbf{I}_3 \otimes \mathbf{S}(\mathbf{n}_{\boldsymbol{\Omega}}(t))$ is a skew-symmetric matrix, straightforward algebraic manipulations allow us then to infer that $\boldsymbol{\mathcal{P}}_{\boldsymbol{\chi}}(t) = \gamma(t)\mathbf{I}$, for all $t \geq t_0$, where $\dot{\gamma}(t) = -\gamma(t)^2/r_3 + r_2$, with $\gamma(t_0) = r_1$, whose solution, for all $t \geq t_0$, can be written as

$$\gamma(t) = \sqrt{r_2 r_3}\frac{\gamma_1 \exp\left(\sqrt{\frac{r_2}{r_3}}t\right) - \gamma_2 \exp\left(-\sqrt{\frac{r_2}{r_3}}t\right)}{\gamma_1 \exp\left(\sqrt{\frac{r_2}{r_3}}t\right) + \gamma_2 \exp\left(-\sqrt{\frac{r_2}{r_3}}t\right)}, \tag{35}$$

where $\gamma_1, \gamma_2 \in \mathbb{R}\backslash\{0\}$ are any constants that satisfy the identity $\gamma_1(\sqrt{r_2 r_3} - r_1) = \gamma_2(\sqrt{r_2 r_3} + r_1)$. This means that we can simplify (34) as

$$\begin{aligned}\dot{V}_{\boldsymbol{\chi}}(t) \leq &-\|\widetilde{\boldsymbol{\chi}}(t)\|^2\left(\frac{r_2}{\gamma(t)^2} + \frac{1}{r_3}\right) + \frac{2\|\mathbf{n}_{\boldsymbol{\chi}}(t)\|}{r_3}\|\widetilde{\boldsymbol{\chi}}(t)\| \\ &+\frac{2\|\mathbf{n}_{\boldsymbol{\Omega}}(t)\|\boldsymbol{\chi}(t)\|}{\gamma(t)}\|\widetilde{\boldsymbol{\chi}}(t)\|.\end{aligned}$$

It follows that $\dot{V}_{\boldsymbol{\chi}}(t) < 0$ for $\|\widetilde{\boldsymbol{\chi}}(t)\| > B_{\boldsymbol{\chi}}(t)$, with

$$B_{\boldsymbol{\chi}}(t) := 2\left(\frac{\|\mathbf{n}_{\boldsymbol{\chi}}(t)\|}{r_3} + \frac{\|\mathbf{n}_{\boldsymbol{\Omega}}(t)\sqrt{3}}{\gamma(t)}\right)\frac{r_3\gamma(t)^2}{\gamma(t)^2 + r_2 r_3},$$

where we took into consideration the fact that, based on the properties of rotation matrices, and in view of (4), it must be $\|\boldsymbol{\chi}(t)\| = \sqrt{3}$ for all $t \geq t_0$. Then, according to (35), we have $\lim_{t\to\infty}\gamma(t) = \sqrt{r_2 r_3}$, which, in turn, implies the existence of an ultimate bound for $\|\widetilde{\boldsymbol{\chi}}(t)\|$ given by

$$\lim_{t\to\infty} B_{\boldsymbol{\chi}}(t) = \|\mathbf{n}_{\boldsymbol{\chi}}(t)\| + \sqrt{3r_3/r_2}\|\mathbf{n}_{\boldsymbol{\Omega}}(t)\|. \tag{36}$$

The results in (35) and (36) are interesting since they establish a (slightly conservative) performance threshold for the estimation accuracy of $\widehat{\boldsymbol{\chi}}$ in function of the gyroscope noise $\mathbf{n}_{\boldsymbol{\Omega}}$, the attitude measurement noise $\mathbf{n}_{\boldsymbol{\chi}}$ and the KF parameters $\boldsymbol{\mathcal{Q}}_{\boldsymbol{\chi}} = r_2\mathbf{I}_9$ and $\boldsymbol{\mathcal{R}}_{\boldsymbol{\chi}} = r_3\mathbf{I}_9$. We note that the convergence of the estimation error is exponential.

A similar analysis can be carried out for the subsystem concerning the state components $\boldsymbol{\omega}$ and $\mathbf{b}_{\boldsymbol{\tau}}$, but it is omitted here due to the lack of space.

5. KALMAN FILTER AIDED CONTROLLER DESIGN

In this section, we will sketch an illustrative nonlinear controller that takes into account the entire KF output given by (28). Consider then the error definitions:

$$\mathbf{e}_{\mathbf{p}}(t) := \mathbf{p}_d(t) - \widehat{\mathbf{p}}(t) + \dot{\mathbf{p}}_d(t) - \widehat{\mathbf{v}}(t) \in \mathbb{R}^3 \text{ and}$$
$$\mathbf{e}_{\boldsymbol{\Omega}}(t) := \widetilde{\mathbf{R}}(t)^\mathsf{T}\boldsymbol{\Omega}_d(t) - \widehat{\boldsymbol{\Omega}}(t) - \text{vex}(\mathbb{P}(\widetilde{\mathbf{R}}(t))) \in \mathbb{R}^3,$$

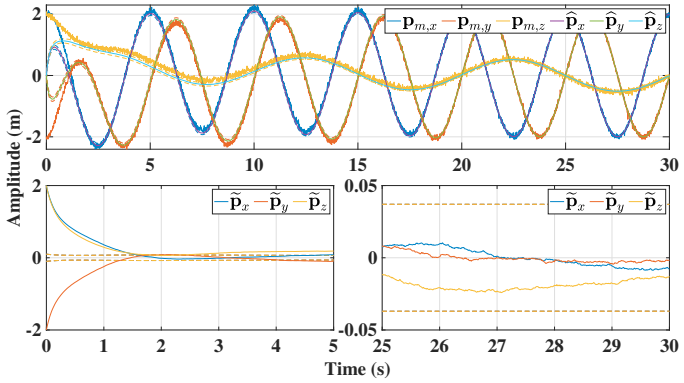

Figure 1. Position smoothing. Top: evolution of $\mathbf{p}_m$ vs. $\widehat{\mathbf{p}}$. Bottom: evolution of $\widetilde{\mathbf{p}} = \mathbf{p} - \widehat{\mathbf{p}}$. Notice the different scales. Dashed lines depict the *1-Sigma*.

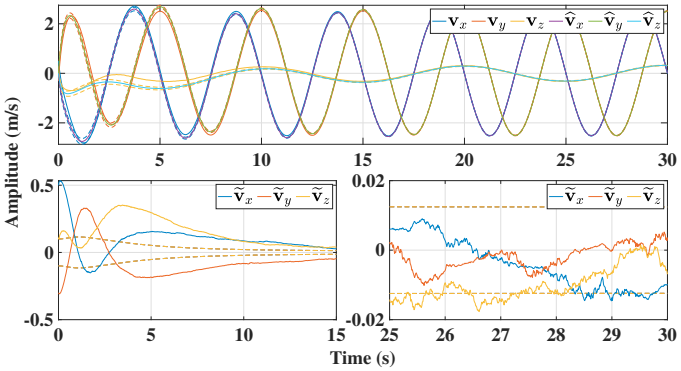

Figure 2. Linear velocity estimation. Top: evolution of $\mathbf{v}$ vs. $\widehat{\mathbf{v}}$. Bottom: evolution of $\widetilde{\mathbf{v}} = \mathbf{v} - \widehat{\mathbf{v}}$. Notice the different scales. Dashed lines depict the *1-Sigma*.

where $\widetilde{\mathbf{R}}(t) := \mathbf{R}_d(t)^\mathsf{T}\widehat{\mathbf{R}}(t) \in \mathsf{SO}(3)$ and $\mathbb{P}(\widetilde{\mathbf{R}}(t)) := (\widetilde{\mathbf{R}}(t) - \widetilde{\mathbf{R}}(t)^\mathsf{T})/2$. Based on (2a), and (2b), let us set the laws for $\mathbf{u}$ in (13), i.e., $\mathbf{f}(t)$ and $\boldsymbol{\tau}(t)$, for all $t \geq t_0$, as

$$\begin{aligned}
&\mathbf{R}(t)\mathbf{f}(t) = \mathbf{e}_\mathbf{p}(t) - \widehat{\mathbf{v}}(t) - \widehat{\mathbf{b}}_\mathbf{v}(t) + \ddot{\mathbf{p}}_d(t) + \dot{\mathbf{p}}_d(t) \\
&- [\mathbf{I}_3 \ \mathbf{I}_3 \ \mathbf{0}_3]\,\boldsymbol{\mathcal{K}}_\mathbf{p}(t)(\mathbf{p}_m(t) - \widehat{\mathbf{p}}(t)) \\
&\mathbf{J}^{-1}\boldsymbol{\tau}(t) = \mathbf{J}^{-1}\mathbf{S}(\boldsymbol{\Omega}_m(t))\mathbf{J}\widehat{\boldsymbol{\Omega}}(t) - \mathbf{J}^{-1}\widehat{\mathbf{b}}_{\boldsymbol{\tau}}(t) + \mathbf{e}_{\boldsymbol{\Omega}}(t) \\
&- \mathbf{J}^{-1}\,[\mathbf{I}_3 \ \mathbf{0}_3]\,\boldsymbol{\mathcal{K}}_{\boldsymbol{\omega}}(t)(\boldsymbol{\Omega}_m(t) - \widehat{\boldsymbol{\Omega}}(t)) \\
&+ \dot{\widetilde{\mathbf{R}}}(t)^\mathsf{T}\boldsymbol{\Omega}_d(t) + \widetilde{\mathbf{R}}(t)^\mathsf{T}\dot{\boldsymbol{\Omega}}_d(t) - \mathrm{vex}(\mathbb{P}(\dot{\widetilde{\mathbf{R}}}(t))).
\end{aligned}$$

By choosing the Lyapunov function $V(t) := 1/2\|\mathbf{e}_\mathbf{p}(t)\|^2 + 1/2\|\mathbf{e}_{\boldsymbol{\Omega}}(t)\|^2$, straightforward algebraic manipulations allow us to conclude that $\dot{V}(t) = -\|\mathbf{e}_\mathbf{p}(t)\|^2 - \|\mathbf{e}_{\boldsymbol{\Omega}}(t)\|^2 < 0$.

6. SIMULATION RESULTS

Consider position and angular velocity references given by $\mathbf{p}_d(t) = [2\cos(2\pi/5t) \ \ 2\sin(2\pi/5t) \ \ 0.5\sin(2\pi/10t)]^\mathsf{T}$ and $\boldsymbol{\Omega}_d(t) = [\cos(t/15) \ \ \sin(t/16) \ \ \cos(t/17)]^\mathsf{T}$, for initial conditions $\mathbf{p}(t_0) = [2 \ 2 \ 2]^\mathsf{T}$, $\mathbf{v}(t_0) = [0.5 \ \ -0.3 \ \ 0.1]^\mathsf{T}$, $\boldsymbol{\Omega}(t_0) = \mathbf{0}$, $\mathbf{R}(t_0) = \mathbf{R}_z(40°)\mathbf{R}_y(-10°)\mathbf{R}_x(80°)$, and $\mathbf{R}_d(t_0) = \mathbf{I}_3$. Let $\mathbf{J} = [2.5 \ 0.5 \ 0.7; 0.5 \ 1.8 \ 1.1; 0.7 \ 1.1 \ 1.7]$ and let the system disturbances be given by $\mathbf{b}_\mathbf{v} = [0.5 \ \ -0.3 \ \ 0.8]^\mathsf{T}$ and $\mathbf{b}_{\boldsymbol{\tau}} = [0.5 \ \ -0.2 \ \ 0.25]^\mathsf{T}$. We set $\widehat{\boldsymbol{\chi}}(t_0) = \mathrm{vec}(\mathbf{I}_3)$; all remaining initial KF estimates are set to zero. Regarding the KF parameters, we choose $\boldsymbol{\mathcal{P}}(t_0) = 10^{-2}\mathbf{I}_{24}$, $\boldsymbol{\mathcal{Q}}_\mathbf{p}(t_0) = 10^{-6}\mathbf{I}_9$, $\boldsymbol{\mathcal{Q}}_{\boldsymbol{\chi}}(t_0) = 10^{-4}\mathbf{I}_9$, $\boldsymbol{\mathcal{Q}}_{\boldsymbol{\omega}}(t_0) = 10^{-4}\mathbf{I}_3$, $\boldsymbol{\mathcal{R}}_\mathbf{p}(t_0) = \sigma_\mathbf{p}^2\mathbf{I}_3$, $\boldsymbol{\mathcal{R}}_{\boldsymbol{\chi}}(t_0) = \sigma_{\boldsymbol{\chi}}^2\mathbf{I}_9$, and $\boldsymbol{\mathcal{R}}_{\boldsymbol{\Omega}}(t_0) = \sigma_{\boldsymbol{\Omega}}^2\mathbf{I}_3$, with $\sigma_\mathbf{p} = 0.05$ (m), $\sigma_{\boldsymbol{\chi}} = 0.015$ and $\sigma_{\boldsymbol{\Omega}} = 0.0175$ (rad/s).

In Figs. 1 through 6, we showcase the results associated with the KF implementation. Notice, in particular, the effective smoothing of noisy measurements, as well as the accurate estimates of linear velocity and external force and torque disturbances. In Fig. 7, we display the results associated with the controller. Notice the expected convergence to zero, as well as the reasonable control inputs, which become increasingly smoother over the transient phase.

7. CONCLUSIONS

We solved the problem of estimating the linear velocity of a rigid-body, in addition to terms of external force and torque disturbances, using noise-filtered pose measurements combined with information about the wrench

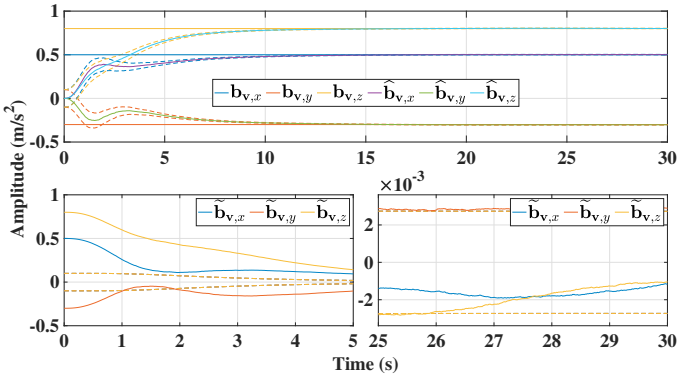

Figure 3. Force disturbance estimation. Top: evolution of $\mathbf{b}_\mathbf{v}$ vs. $\widehat{\mathbf{b}}_\mathbf{v}$. Bottom: evolution of $\widetilde{\mathbf{b}}_\mathbf{v} = \mathbf{b}_\mathbf{v} - \widehat{\mathbf{b}}_\mathbf{v}$. Notice the different scales. Dashed lines depict the *1-Sigma*.

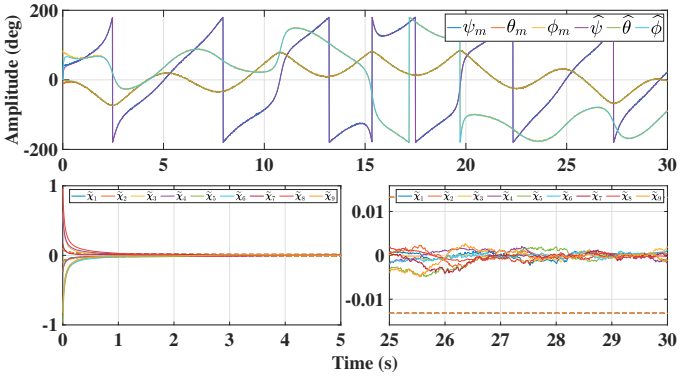

Figure 4. Attitude smoothing. Top: evolution of measured vs. estimated Euler angles (yaw ψ, pitch θ and roll ϕ). Bottom: evolution of $\widetilde{\boldsymbol{\chi}} = \boldsymbol{\chi} - \widehat{\boldsymbol{\chi}}$. Notice the different scales. Dashed lines depict the *1-Sigma*.

applied to the center of mass of a rigid-body. By designing an LTV system, with no linearizations involved, a Kalman filter (KF) was employed which, on account of the system being uniformly completely observable, renders the total estimation error globally exponentially stable. Realistic simulation results using a KF-aided nonlinear pose tracking controller were presented to validate and showcase the performance of the proposed methodology.

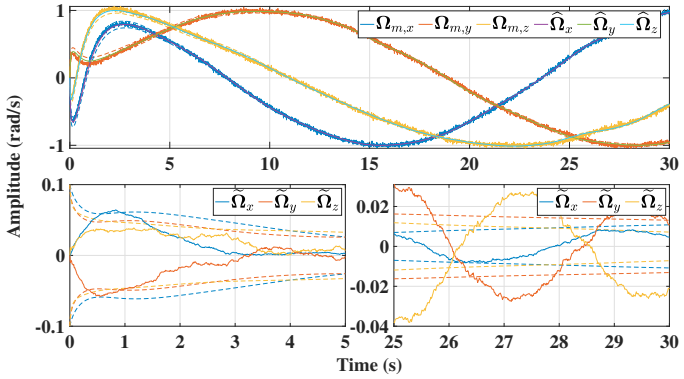

Figure 5. Angular velocity smoothing. Top: evolution of $\boldsymbol{\Omega}_m$ vs. $\widehat{\boldsymbol{\Omega}}$. Bottom: evolution of $\widetilde{\boldsymbol{\Omega}} = \boldsymbol{\Omega} - \widehat{\boldsymbol{\Omega}}$. Notice the different scales. Dashed lines depict the *1-Sigma*.

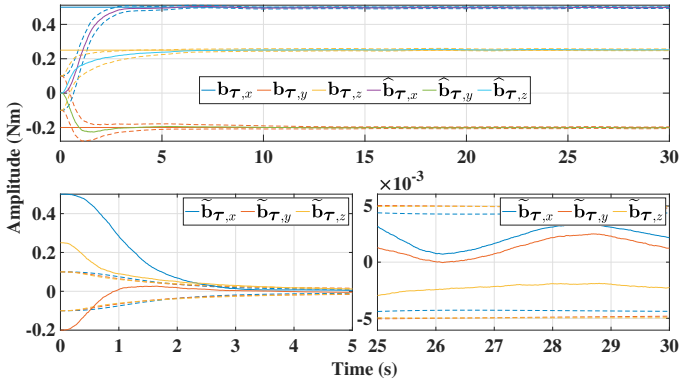

Figure 6. Torque disturbance estimation. Top: evolution of $\mathbf{b}_{\boldsymbol{\tau}}$ vs. $\widehat{\mathbf{b}}_{\boldsymbol{\tau}}$. Bottom: evolution of $\widetilde{\mathbf{b}}_{\boldsymbol{\tau}} = \mathbf{b}_{\boldsymbol{\tau}} - \widehat{\mathbf{b}}_{\boldsymbol{\tau}}$. Notice the different scales. Dashed lines depict the *1-Sigma*.

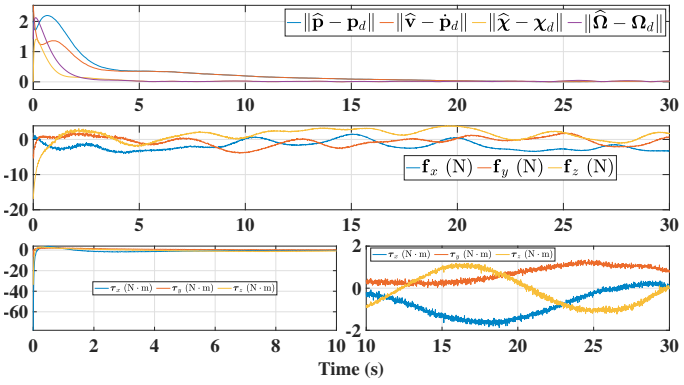

Figure 7. Top: evolution of control errors. Center: evolution of force input $\mathbf{f}$. Bottom: evolution of torque input $\boldsymbol{\tau}$.

REFERENCES

Afonin, A.A., Mikhaylin, D.A., Sulakov, A.S., and Moskalev, A.P. (2020). The Adaptive Kalman Filter in Aircraft Control and Navigation Systems. In *2020 2nd International Conference on Control Systems, Mathematical Modeling, Automation and Energy Efficiency (SUMMA)*. IEEE. doi:10.1109/summa50634.2020.9280720.

Aravkin, A., Burke, J.V., Ljung, L., Lozano, A., and Pillonetto, G. (2017). Generalized Kalman smoothing: Modeling and algorithms. *Automatica*, 86, 63–86. doi:10.1016/j.automatica.2017.08.011.

Barrau, A. and Bonnabel, S. (2017). The Invariant Extended Kalman Filter as a Stable Observer. *IEEE Transactions on Automatic Control*, 62(4), 1797–1812. doi:10.1109/tac.2016.2594085.

Batista, P., Silvestre, C., and Oliveira, P. (2011). On the observability of linear motion quantities in navigation systems. *Systems & Control Letters*, 60(2), 101–110. doi:10.1016/j.sysconle.2010.11.002.

Brockett, R.W. (2015). *Finite Dimensional Linear Systems*. Society for Industrial and Applied Mathematics. doi:10.1137/1.9781611973884.

Chrif, L. and Kadda, Z.M. (2014). Aircraft Control System Using LQG and LQR Controller with Optimal Estimation-Kalman Filter Design. *Procedia Engineering*, 80, 245–257. doi:10.1016/j.proeng.2014.09.084.

Fareh, R., Khadraoui, S., Abdallah, M.Y., Baziyad, M., and Bettayeb, M. (2021). Active disturbance rejection control for robotic systems: A review. *Mechatronics*, 80, 102671. doi:10.1016/j.mechatronics.2021.102671.

Jazwinski, A.H. (1970). *Stochastic processes and filtering theory*. Number v. 64 in Mathematics in science and engineering. Academic Press, New York. Includes bibliographies and index.

Kalman, R.E. (1960). A New Approach to Linear Filtering and Prediction Problems. *Journal of Basic Engineering*, 82(1), 35–45. doi:10.1115/1.3662552.

Mangiacapra, G., Wittal, M., Capello, E., and Nazari, M. (2022). Unscented Kalman filter and control on TSE(3) with application to spacecraft dynamics. *Nonlinear Dynamics*, 108(3), 2127–2146. doi:10.1007/s11071-022-07293-x.

Markley, F.L. and Sedlak, J.E. (2008). Kalman Filter for Spinning Spacecraft Attitude Estimation. *Journal of Guidance, Control, and Dynamics*, 31(6), 1750–1760. doi:10.2514/1.35221.

Moakher, M. (2002). Means and Averaging in the Group of Rotations. *SIAM Journal on Matrix Analysis and Applications*, 24(1), 1–16. doi:10.1137/s0895479801383877.

Schmidt, S.F. (1981). The Kalman filter - Its recognition and development for aerospace applications. *Journal of Guidance and Control*, 4(1), 4–7. doi:10.2514/3.19713.

Shuster, M. (1989). A simple Kalman filter and smoother for spacecraft attitude. *Journal of the Astronautical Sciences*, 37(1), 89–106.

Simon, D. (2006). *Optimal State Estimation: Kalman, H∞, and Nonlinear Approaches*. Wiley. doi:10.1002/0470045345.

Urrea, C. and Agramonte, R. (2021). Kalman Filter: Historical Overview and Review of Its Use in Robotics 60 Years after Its Creation. *Journal of Sensors*, 2021, 1–21. doi:10.1155/2021/9674015.

Vouch, O., Nardin, A., Minetto, A., Zocca, S., Valvano, M., and Dovis, F. (2024). Aided Kalman Filter Models for GNSS-Based Space Navigation. *IEEE Journal of Radio Frequency Identification*, 1–1. doi:10.1109/jrfid.2024.3403914.

Zarei, J., Montazeri, A., Reza Jahed Motlagh, M., and Poshtan, J. (2007). Design and comparison of LQG/LTR and H∞ controllers for a VSTOL flight control system. *Journal of the Franklin Institute*, 344(5), 577–594. doi:10.1016/j.jfranklin.2006.02.033.